2017

Enhanced rate-capability and cycling-stability of 5 V SiO2- and polyimide-coated cation ordered LiNi0.5Mn1.5O4 lithium-ion battery positive electrodes

Wei Kong Pang
University of Wollongong, wkpang@uow.edu.au

Hsiu-Fen Lin
National Formosa University

Vanessa K. Peterson
University of Wollongong

Cheng-Zhang Lu
Industrial Technology Research Institute, Taiwan

Chia-Erh Liu
Industrial Technology Research Institute, Taiwan

See next page for additional authors

Publication Details

Pang, W., Lin, H., Peterson, V. K., Lu, C., Liu, C., Liao, S. & Chen, J. (2017). Enhanced rate-capability and cycling-stability of 5 V SiO2- and polyimide-coated cation ordered LiNi0.5Mn1.5O4 lithium-ion battery positive electrodes. The Journal of Physical Chemistry C: Energy Conversion and Storage, Optical and Electronic Devices, Interfaces, Nanomaterials, and Hard Matter, 121 (7), 3680-3689.

Enhanced rate-capability and cycling-stability of 5 V SiO2- and polyimide-coated cation ordered LiNi0.5Mn1.5O4 lithium-ion battery positive electrodes

Abstract

The ordered LiNi0.5Mn1.5O4 spinel exhibits great promise as a potential high-energy positive electrode for lithium-ion batteries due to its exceptionally high working potential of 4.7 V (vs. Li) and energy density of 640 Wh kg-1. The commercial application of this material at such voltages is unfortunately prevented by reaction phenomena including hydrofluoric acid attack and manganese dissolution, as well as the two-phase mechanism of Li insertion and extraction, with these limiting Li diffusivity and cycling stability. In this work, we demonstrate the improved performance of LiNi0.5Mn1.5O4 achieved by encapsulating the material in a thin layer of silica (SiO2) or polyimide using a simple wet-chemical method and organic solvents. The pristine and coated ordered LiNi0.5Mn1.5O4 spinel are both confirmed to have P4332 symmetry, with only a minor difference in their lattice parameter. The SiO2 coating is found to reduce capacity fade of ordered LiNi0.5Mn1.5O4 by 45 and 65% at 25 and 55 °C, respectively, with the improvement attributed to enhanced Li diffusivity alongside the suppression of the hydrofluoric acid attack. The polyimide coating is found to have a marginally negative effect on both capacity and rate performance of ordered LiNi0.5Mn1.5O4, with this being greatly offset by excellent thermal stability leading to high-temperature protection, with the material having the low capacity fade of 0.0585 mAh g-1 cycle-1 at 55 °C, which is comparable to that at 25 °C. While similar effects of these coatings are found for disordered LiNi0.5Mn1.5O4, the magnitude of enhancement to properties offered by these coatings is significantly lesser than those found here for the ordered LiNi0.5Mn1.5O4. A stabilizing effect of the coatings that mitigates against phase segregation occurring during the additional two-phase reaction in the ordered but not the disordered phase of the material may explain the greater benefit of the coatings to the ordered phase.

Disciplines

Engineering | Physical Sciences and Mathematics

Publication Details

Pang, W., Lin, H., Peterson, V. K., Lu, C., Liu, C., Liao, S. & Chen, J. (2017). Enhanced rate-capability and cycling-stability of 5 V SiO2- and polyimide-coated cation ordered LiNi0.5Mn1.5O4 lithium-ion battery positive electrodes. The Journal of Physical Chemistry C: Energy Conversion and Storage, Optical and Electronic Devices, Interfaces, Nanomaterials, and Hard Matter, 121 (7), 3680-3689.

Authors

Wei Kong Pang, Hsiu-Fen Lin, Vanessa K. Peterson, Cheng-Zhang Lu, Chia-Erh Liu, Shih-Chieh Liao, and Jin-Ming Chen

Enhanced Rate-Capability and Cycling-Stability of 5 V SiO_2- and Polyimide-Coated Cation Ordered $LiNi_{0.5}Mn_{1.5}O_4$ Lithium-Ion Battery Positive Electrodes.

Wei Kong Pang,[1,2,] Hsiu-Fen Lin,[3] Vanessa K. Peterson,[1,2,*] Cheng-Zhang Lu,[4] Chia-Erh Liu,[4] Shih-Chieh Liao,[4] Jin-Ming Chen[4]*

[1] Australian Centre for Neutron Scattering, Australian Nuclear Science and Technology Organization, Locked Bag 2001, Kirrawee DC, NSW 2232, Australia.

[2] Institute for Superconducting & Electronic Materials, Faculty of Engineering, University of Wollongong, NSW 2522, Australia.

[3] Department of Materials Science and Engineering, National Formosa University, Yunlin County 63201, Taiwan.

[4] Department of Energy Nanomaterials, Material & Chemical Research Laboratory, Industrial Technology Research Institute, Taiwan.

*Corresponding authors.

Abstract

The ordered $LiNi_{0.5}Mn_{1.5}O_4$ spinel exhibits great promise as a potential high-energy positive electrode for lithium-ion batteries due to its exceptionally-high working potential of 4.7 V (*vs*. Li) and energy density of 640 Wh kg^{-1}. The commercial application of this material at such voltages is unfortunately prevented by reaction phenomena including hydrofluoric acid attack and manganese dissolution, as well as the two-phase mechanism of Li insertion and extraction, with these limiting Li diffusivity and cycling stability. In this work, we demonstrate the improved performance of $LiNi_{0.5}Mn_{1.5}O_4$ achieved by encapsulating the material in a thin layer of silica (SiO_2) or polyimide using a simple wet-chemical method and organic solvents. The pristine and coated ordered $LiNi_{0.5}Mn_{1.5}O_4$ spinel are both confirmed to have $P4_332$ symmetry, with only a minor difference in their lattice parameter. The SiO_2 coating is found to reduce capacity fade of ordered $LiNi_{0.5}Mn_{1.5}O_4$ by 45 and 65% at 25 and 55 °C, respectively, with the improvement attributed to enhanced Li diffusivity alongside the suppression of the hydrofluoric acid attack. The polyimide coating is found to have a marginally negative effect on both capacity and rate performance of ordered $LiNi_{0.5}Mn_{1.5}O_4$, with this being greatly offset by excellent thermal stability leading to high-temperature protection, with the material having the low capacity fade of 0.0585 mAh g^{-1} $cycle^{-1}$ at 55 °C, which is comparable to that at 25 °C. Whilst similar effects of these coatings are found for disordered $LiNi_{0.5}Mn_{1.5}O_4$, the magnitude of enhancement to properties offered by these coatings is significantly lesser than those found here for the ordered $LiNi_{0.5}Mn_{1.5}O_4$. A stabilizing effect of the coatings that mitigates against phase segregation occurring during the additional two-phase reaction in the ordered but not the disordered phase of the material may explain the greater benefit of the coatings to the ordered phase.

■ INTRODUCTION

Lithium-ion batteries (LIBs) are the major power source for portable electronic devices as well as for electric automotive applications since the introduction of the technology by Sony Tech. in 1991.[1] Of the large number of positive electrode materials researched in the past two decades, only layered oxides with $R\bar{3}m$ symmetry (i.e., $LiCoO_2$)[2], spinel oxides with $Fd\bar{3}m$ symmetry (i.e., $LiMn_2O_4$)[3], and olivine-like poly-anion oxides with *Pnma* symmetry (i.e., $LiFePO_4$)[4-5], are commercially used in LIBs, mainly due to their exceptional cycling ability and reasonably-high energy/power density.[6-8] However, both existing and emerging technology require LIBs with energy and power capabilities that are beyond the existing state-of-the-art.

Improvement in battery energy density is commonly achieved by raising the battery working voltage, for example, to 5 V. The more widely studied high-voltage positive electrode materials for LIBs include NMC-type layered oxides such as Li-rich Li_2MnO_3, mixed manganese-based spinels, and Ni- or Co-based poly-anions.[9] With a high intercalation working voltage of ~ 4.7 V *vs*. Li, high rate capability, high energy density, good safety, and low environmental impact, the mixed manganese-based spinel materials such as $LiNi_{0.5}Mn_{1.5}O_5$ (LNMO), are considered the most promising for high-energy-density (640 mWh g^{-1}) LIB application.[10-11] However, the cycle life of such materials is insufficient for practical application, and increasing cycling performance has been the focus of intense recent research, with the main hurdles being the instability of conventional organic carbonate-based electrolytes (> 4.3 V vs. Li)[12-17] at high voltage and the existence of two-phase reaction behavior.[18-20]

The high voltage deterioration of the electrolyte induces the formation of a solid-electrolyte interphase (SEI) layer with low lithium conductivity at the positive electrode, leading to growing

electrochemical impedance and poor cycling performance, as well as rate capability.[21-22] Further, electrolyte decomposition causes the formation of hydrofluoric acid which corrodes the electrode and accelerates the dissolution of manganese into the remaining electrolyte *via* disproportionation of Mn^{3+}, decreasing the amount of active positive electrode.[17]

LNMO can exist as either a $P4_332$ symmetry phase with ordered cationic arrangements of Li^+ at the 8*c* site, Ni^{2+} at the 4*b* site, and Mn^{4+} at the 12*d* site, or a face-centered $Fd\bar{3}m$ symmetry phase in which cations are not ordered and 16*d* sites are shared by Ni^{2+} and Mn^{4+} and 8*a* sites are occupied by Li^+.[18-19, 23-24] For clarity, we term the $P4_332$ ordered and $Fd\bar{3}m$ disordered phases P-LNMO and F-LNMO, respectively. Both phases have similar theoretical capacities, good capacity retention, high coulombic efficiency, as well as good charge-discharge performance. The P-LNMO phase undergoes two cubic-cubic two-phase reactions upon charging, accompanied by a ~ 6% change in lattice volume[2] and the F-LNMO phase has either a single-phase or solid-solution and two-phase reaction sequence on charging, with these associated with the Ni^{2+}/Ni^{3+} and Ni^{3+}/Ni^{4+} redox couples, respectively.[18] It is generally accepted that F-LNMO exhibits better charge-discharge and cycling capability than the P-LNMO, due to higher electronic conductivity (10^{-7} vs. $10^{-4.5}$ S cm^{-1})[25], lithium diffusivity (D_{Li} ~ 3×10^{-13} cm^2 s^{-1} at the upper 4.7 V Ni^{3+}/Ni^{4+} plateau, ~ 3×10^{-12} cm^2 s^{-1} at the lower 4.7 V Ni^{2+}/Ni^{3+} plateau, and 5×10^{-11} cm^2 s^{-1} at the 4.0 V Mn^{3+}/Mn^{4+} redox plateau *vs*. ~ 3×10^{-13} cm^2 s^{-1} for P-LNMO)[26], and lower impedance.[27] The higher electronic conductivity is thought to arise from increased electron hopping as a result of higher Mn^{3+} content[25] and the larger D_{Li} is believed to arise from differences in single- and two-phase reactions. The two-phase region in F-LNMO has a similar D_{Li} to that in P-LNMO, but lithium certainly has a significantly greater diffusivity during the single-phase transitions, as the two-phase separation induces unfavorable inter-grain stress that

results in grain breakdown, phase bordering, and phase interface movement.[10] Overall, F-LNMO has a larger lithium diffusion coefficient and has a Ni^{2+}/Ni^{3+} single-phase transition which results in higher structural reversibility, especially at high rates, than P-LNMO.[24, 28] Despite the superior properties of F-LNMO, P-LNMO is still of interest to both researchers and engineers because of the lower preparation temperature, leading to lower cost, and its monotonic redox plateau feature, leading to ease of battery design.

Surface modification has proven to be one of the most effective ways to positively influence the electrochemical performance of electrodes as well as to protect them from acid attack in LIBs. Certain metal oxides and carbon, such as Al_2O_3[29], $AlPO_4$[30], Bi_2O_3[31], SiO_2[32], ZnO[33], $Li_4P_2O_7$,[34] graphene oxides[35], solid-electrolyte compounds[36], etc., have been employed to improve the cycling performance of LNMO through the suppression of hydrofluoric acid attack and Mn dissolution. Such coatings are usually distributed on the particle surface non-uniformly. SiO_2[37] and polyimide (PI)[38] coatings, generated from organic compounds, come with outstanding mechanical, thermal, and chemical stability, and have also been used as coatings to protect LNMO, with these improving electrochemical, particularly during high voltage charging. Moreover, given that the Li diffusivity at the electrode-electrolyte interface is estimated to be about 10^{-8} cm^2 s^{-1} and therefore not the rate determining factor,[39] a thin coating of such materials is not expected to hinder significantly Li diffusion. It has been reported that the coated F-LNMO delivers enhanced cycling ability and capacity performance, comparable to that for uncoated F-LNMO.[32, 38, 40] The capacity retention of F-LNMO is enhanced by ~ 46% with a SiO_2 coating,[32] and PI-coated F-LNMO has superior cycling performance at 55 °C to the uncoated material.[38, 40] In this work we synthesized P-LNMO and studied the effects of both SiO_2 and PI coatings on the electrochemical performance of the material as a LIB positive electrode.

■ EXPERIMENTAL

P-LNMO powders were synthesized by a co-precipitation method. An aqueous solution of $NiSO_4 \cdot 6H_2O$ and $MnSO_4 \cdot H_2O$ was slowly pumped into a reactor at 50 °C. Simultaneously, aqueous solutions of NH_4OH and NaOH were fed into the solution to maintain pH at 10.5. $Ni_{0.25}Mn_{0.75}(OH)_2$ precursor with particle diameter ~ 10 – 15 μm was obtained from the co-precipitation process and mixed with lithium carbonate (Li_2CO_3) powder before calcining in air at 750 °C for 12 h to obtain LNMO.

The as-prepared powders were separated evenly into 3 portions with one serving as pristine P-LNMO. One portion was coated with SiO_2 and the other with PI. To coat SiO_2 on the P-LNMO powder, tetraethyl orthosilicate (TEOS) was used and mixed with the LNMO powder in ethanol at room temperature under constant stirring for 3 h, forming a mud-like mixture after filtration following the removal of excess ethanol and unreacted solids. The collected material was dried in an oven at 50 – 100 °C for 10 min followed by baking at 300 – 500 °C for 5 h in air, to obtain the electrode powder encapsulated with a SiO_2 nano-coating. To coat PI on P-LNMO, dimethyl-acetamide was used as a solvent to mix 26 wt.% pyromellitic dianhydride, 10 wt.% p-phenylenediamine, 35.5 wt.% biphenyl dianhydride, and 28.5 wt.% oxydianiline with the P-LNMO powder. 3 wt.% of polyamic acid (PAA) in P-LNMO was added to the solution mix and stirred for 30 min. The wet powders were filtered and dried at 40 °C for 3 h under vacuum. The obtained P-LNMO mixture with PAA was then cured at 60, 120, 150, 200, 300, and finally 400 °C, under nitrogen for 1 h at each step to obtain PI-coated P-LNMO.

X-ray powder diffraction (XRPD) and high-resolution neutron powder diffraction (NPD) data were collected using an X'pert Pro with Cukα radiation and ECHIDNA, the high-resolution

neutron powder diffractometer with 1.6214(4) Å neutrons (determined using the $La^{11}B_6$ NIST standard reference material 660b) at the Open Pool Australian Light-water (OPAL) research reactor at the Australian Nuclear Science and Technology Organisation (ANSTO).[41] XRPD data were collected over the 2θ range of 10 – 80° with a step size of 0.02° and NPD data were obtained over the 2θ range 6.5 – 164° with a step size of 0.05°. GSAS-II[42] was employed to perform Rietveld analysis of the high-resolution NPD data. The refineable parameters included the background coefficients, zero-shift, peak shape parameters, lattice parameters, atomic positional parameters, isotropic atomic displacement parameters (U_{iso}), and site occupancies of Ni and Mn. The morphology of the as-synthesized samples was investigated using field-emission scanning electron microscopy (FE-SEM) with a Hitachi SU8000 operated at 15 keV and transmission electron microscopy (TEM) with a JEOL JEM-2010F at 200 keV. All observations were carried out without applying a conductive coating and with a 10 kV acceleration voltage. The particle size distribution of the as-prepared samples was examined using a DLS particle size analyzer.

P-LNMO electrodes were fabricated by mixing active material powders with conductive carbon (Super P) and polyvinylidene difluoride (PVDF) binder in a weight ratio of 92:4:4 in an adequate amount of N-methyl-2-pyrrolidone. The blended slurry was coated onto aluminum foil and then dried at 80 °C for 1 h to evaporate the organic solvent. The coated foil was roll-pressed and dried at 100 °C for 12 h in a vacuum furnace to obtain the electrode. The electrodes were assembled into CR2032-type coin cells with Li metal as the counter electrode and 1 M $LiPF_6$ dissolved in a 1:1 mixture by volume of ethylene carbonate (EC) and dimethyl carbonate (DMC) as the electrolyte for electrochemical characterization. The coin cells were assembled in a glove box under an argon atmosphere and the electrochemical instrument (Maccor series 4000, USA)

was employed to perform electrochemical tests at 25 and 55 °C within the voltage window 3.5 - 4.9 V (*vs*. Li). Four-point probe measurements using Ohm-Meter DV-5011 (Delta United Instrument Co., Ltd. Taiwan) were performed to determine the electrical conductivity and resistivity of pristine and coated LNMO electrodes. Electrochemical impedance spectroscopy (EIS) and AC impedance of fresh and cycled cells was measured at equilibrium under the full-discharged state in the frequency range 100 kHz to 0.01 Hz using a galvanostat (AutoLab PGSTAT30, Eco Chemie B.V., Netherlands). To test the protective effect of coatings against electrolyte attack, cycled Li electrodes were extracted from disassembled coin cells and washed with anhydrous DMC in a glove box under an argon atmosphere. Each Li electrode was then dissolved in a 5 mL 2 wt.% HNO_3 solution and the Mn content in each solution was measured using inductively coupled plasma atomic emission spectrometry (ICP-AES, Optima 7000DV, Perkin Elmer).

■ RESULTS AND DISCUSSION

This work aims to enhance the performance of P-LNMO when used as a high-energy LIB positive electrode and to study the effects of SiO_2 and PI coatings on its electrochemical properties. Due to the similar lattice parameters of the P-LNMO and F-LNMO phases and the relatively-low sensitivity of X-rays towards Li ions in the presence of heavier elements such as Ni and Mn, the XRPD data are unable to confirm the phase structure of the as-prepared samples and distinguish the P-LNMO and F-LNMO phases. The XRPD patterns of the samples are shown in **Figure S1** in the Supporting Information. NPD data were used to determine the crystallographic details of pristine, SiO_2-coated, and PI-coated P-LNMO. All samples adopt the spinel form with $P4_332$ symmetry, indicating that the coating processes do not significantly

change the material's structure. The refinement profiles are shown in **Figure 1** and crystallographic details obtained from Rietveld analysis are given in **Table 1**, indicating similar crystallographic features between pristine and coated P-LNMO powders in this work. The Ni/Mn ordering proceeds slowly at 700 °C and the degree of ordering is controllable through the isothermal annealing time.[19] It is notable that the annealing temperature used in this work was 750 °C and the dwell time was 12 h, which is 50 °C higher than the generally-accepted sintering temperature enabling P-LNMO to be exclusively obtained, where F-LNMO generally forms at temperatures above 800 – 1000 °C. Our syntheses suggest that an annealing temperature of 750 °C and 12 h dwell time produce the desired LNMO form. Higher annealing temperatures can cause the LNMO to decompose into a rock-salt phase $Li_xNi_{1-x}O$ as metal-oxygen bonds are broken, inducing oxygen vacancies and resulting in a higher Mn^{3+} content.[19, 24] Although the secondary rock-salt phase $Li_xNi_{1-x}O$ is expected not to impact negatively on cycling performance, it reduces capacity of the electrode.[43]

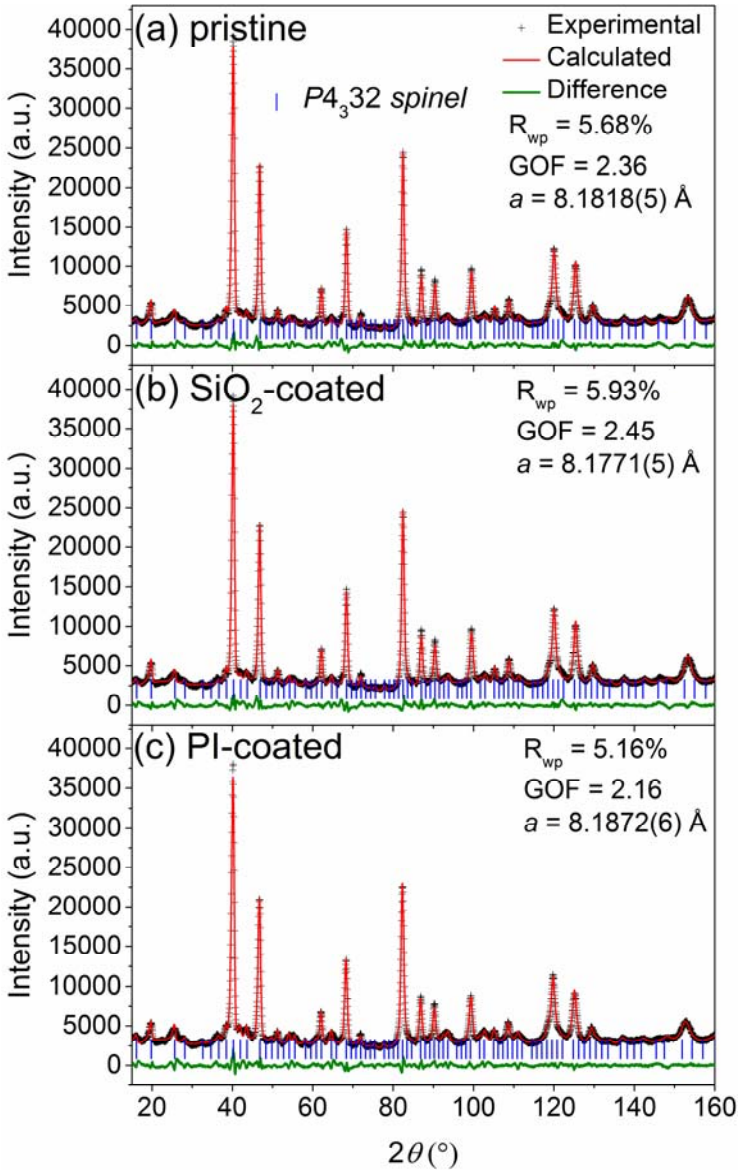

Figure 1. Rietveld refinement profiles using high-resolution NPD data for (a) pristine, (b) SiO_2-coated, and (c) PI-coated P-LNMO. Data are shown as crosses and the calculation is the red solid line. The difference between the measured and calculated patterns is shown as a green line along the bottom of the plots. Vertical bars represent the reflection positions.

Table 1. Crystallographic details of pristine and coated LNMO obtained from Rietveld analysis using high-resolution NPD data.

Pristine $LiNi_{0.5}Mn_{1.5}O_4$

Space group = $P4_332$

a = 8.1817(5) Å, Vol. = 547.70(4) $Å^3$, R_F^2 = 2.36%

Atom	Site	*x*	*y*	*z*	U_{iso} ($Å^2$)	Site occupancy factor
Mn	12*d*	0.125	0.380()	0.870(1)	0.0050(4)***	0.866(2)^
Ni	12*d*					0.134(2)^
Mn	4*b*	0.625	0.625	0.625	0.0050(4)***	0.460(4)^^
Ni	4*b*					0.540(4)^^
Li	8*c*	-0.005(1)*	-0.005(1)*	-0.005(1)*	0.0050(4)***	1
O	8*c*	0.3844(4)**	0.3844(4)**	0.3844(4)**	0.0050(4)***	1
O	24*e*	0.1402(4)	0.8581(3)	0.1347(3)	0.0050(4)***	1

SiO_2-coated $LiNi_{0.5}Mn_{1.5}O_4$

Space group = $P4_332$

a = 8.1771(6) Å, Vol. = 546.77(4) $Å^3$, R_F^2 = 2.76%

Atom	Site	*x*	*y*	*z*	U_{iso} ($Å^2$)	Site occupancy factor
Mn	12*d*	0.125	0.3823(7)	0.8677(7)	0.0046(5)***	0.909(2)^
Ni	12*d*					0.091(2)^
Mn	4*b*	0.625	0.625	0.625	0.0046(5)***	0.377(3)^^
Ni	4*b*					0.623(3)^^
Li	8*c*	-0.002(1)*	-0.002(1)*	-0.002(1)*	0.0046(5)***	1
O	8*c*	0.3855(3)**	0.3855(3)**	0.3855(3)**	0.0046(5)***	1
O	24*e*	0.1427(3)	0.8599(3)	0.1330(3)	0.0046(5)***	1

PI-coated $LiNi_{0.5}Mn_{1.5}O_4$ Space group = $P4_332$ a = 8.1871(6) Å, Vol. = 548.78(4) $Å^3$, R_F^2 = 2.59%						
Atom	Site	x	y	z	U_{iso} ($Å^2$)	Site occupancy factor
Mn	12*d*	0.125	0.3837(8)	0.8663(8)	0.0052(5)***	0.911(3)^
Ni	12*d*					0.089(3)^
Mn	4*b*	0.625	0.625	0.625	0.0052(5)***	0.382(4)^^
Ni	4*b*					0.618(4)^^
Li	8*c*	-0.002(1)*	-0.002(1)*	-0.002(1)*	0.0052(5)***	1
O	8*c*	0.3857(3)**	0.3857(3)**	0.3857(3)**	0.0052(5)***	1
O	24*e*	0.1426(3)	0.8598(3)	0.1322(3)	0.0052(5)***	1

^, ^^ constrained to sum to unity, *, **,*** constrained to be the same.

The effects of coating processes on the P-LNMO morphology were examined using SEM and TEM. As shown in **Figure 2a**, SEM reveals that the P-LNMO was highly aggregated, with particle size 5 – 20 μm in diameter. The particle-size distribution, d (0.5), was also determined to be ~ 16.6 μm (shown in **Figure S2**). The narrow particle-size distribution may be attributed to the co-precipitation procedure that involves the preparation of a homogeneous precursor solution. The SiO_2-coated P-LNMO (**Figure 2b**) aggregates were more spherical than the pristine material, with a macroporous morphology composed of 0.5 – 1 μm particles fused together. This was likely caused by the reaction with TEOS and the removal of unreacted material. A complete SiO_2 coating is found, encapsulating the P-LNMO particles with a thickness of 5 – 20 nm. The formed SiO_2 film on the P-LNMO particle surface protects the particle from hydrofluoric acid attack and avoids the dissolution of Mn, as well as exhibiting

"open" channels for small positive ions such as Li^+ and Na^+ to migrate through. The electrical conductivities of pristine and coated LNMO electrodes, obtained using four-point probe measurements, and are listed in Table S1. These confirm that the coatings do affect the electrical resistivity of the samples, with the electric conductivity being ~ 8.3% enhanced by the thin silica layer and ~ 1.9% reduced by the PI coating. Further, the electric conductivity of the thin silica layer will be enhanced by Li+ present in the internal structure following cycling, and therefore the SiO2 nano-layer is expected to be electronically conductive[32] and unlikely to negatively impact ionic conductivity. SEM images of the PI-coated P-LNMO (**Figure 2c**) reveal spherical aggregates that consist of irregular rod-like particles. The PI coating is found to not completely cover the surface, being distributed randomly in small sections. As indicated by the measured conductivity, the insulating property of the PI coating does not significantly affect electrical conductivity, and is postulated to suppress the dissolution of Mn by reducing contact between the P-LNMO particle and the electrolyte. Given that the particle size of the P-LNMO remained nearly unchanged after coating with PI, it is the dissimilar morphology of the aggregates, as well as the coating layer, that is expected to affect electrochemical performance of this P-LNMO.

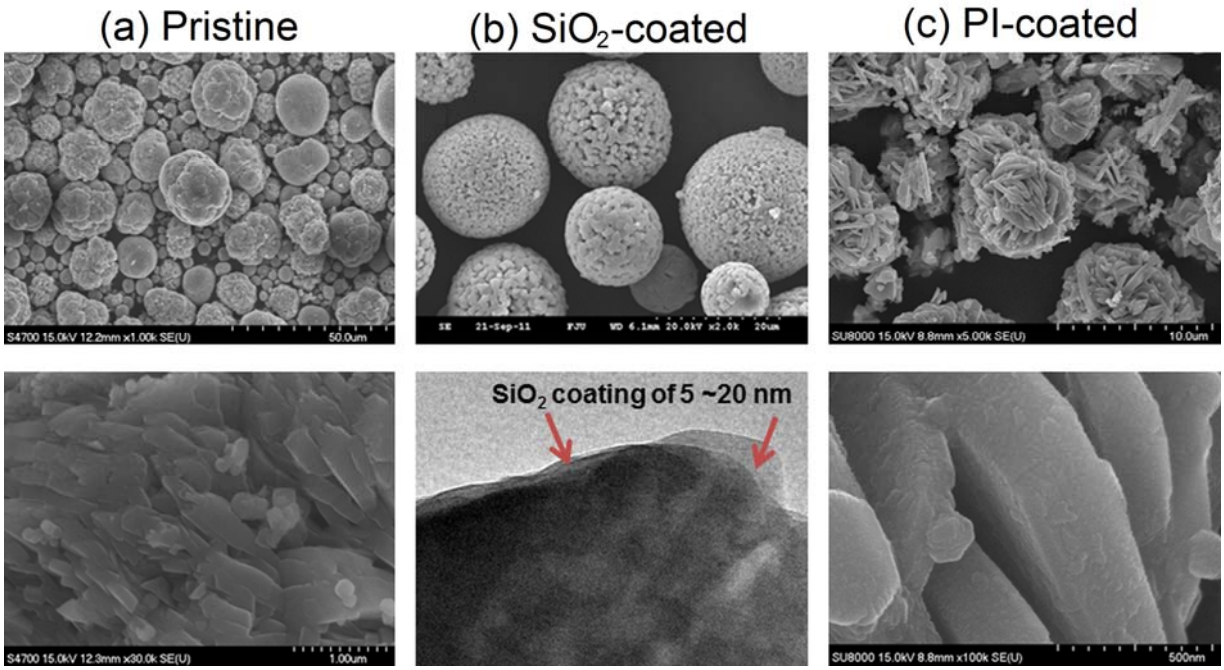

Figure 2. FE-SEM images at low (top) and high (bottom) magnification of pristine and coated P-LNMO particles. The high-magnification SEM image of SiO_2-coated P-LNMO is replaced with a high-resolution TEM image, showing the SiO_2 coating layer on the particle.

The electrochemical performance of the coated and pristine P-LNMO was tested in coin-type cells. **Figure 3a** shows the first charge-discharge curve of cells containing pristine and coated P-LNMO electrodes and **Figure 3b** shows the corresponding incremental capacity plot for these. For the cell prepared with pristine P-LNMO, two oxidation peaks at 4.73 and 4.77 V, and two overlapped reduction peaks, at 4.70 and 4.65 V, corresponding to Ni^{2+}/Ni^{3+} and Ni^{3+}/Ni^{4+} redox couples, respectively, are observed in the first cycle. The absence of the 4 V plateau (attributed to the Mn^{3+}/Mn^{4+} redox couple) indicates that no oxygen vacancies are present in the pristine P-LNMO. For the SiO_2-coated P-LNMO, in addition to the nearly invisible 4 V plateau, the two oxidation peaks are located at 4.72 and 4.76 V, where the broad reduction peak is positioned at 4.70 V. These lower oxidation and higher reduction potential confirm a smaller voltage

polarization, indicating better energy efficiency of the SiO_2-coated P-LNMO. This is probably due to enhanced ionic and electric conductivities offered by the nano-SiO_2 coating. In contrast, PI-coated P-LNMO exhibits a 4 V plateau with significant peak current, a broad oxidation peak centered at 4.76 V, and a broad reduction peak at 4.70 V. Although the polarization of the high-voltage redox couple is smaller, the 4 V plateau lowers the overall energy density. Although the NPD results revealed all P-LNMO samples to have a spinel structure with $P4_332$ symmetry, the charge-discharge curves of the PI-coated P-LNMO material exhibit a 4.0 V plateau, corresponding to the Mn^{3+}/Mn^{4+} redox reaction and indicating the existence of Mn^{3+} prior to charging. This is somewhat in conflict with the NPD results which show that only F-LNMO contains oxygen vacancies. This discrepancy is believed to arise from the post-processing of PI-coated P-LNMO during coating, where the annealing of organic compounds in a nitrogen atmosphere leads to the reduction of Mn^{4+} to Mn^{3+}, but does not change the structural symmetry as the temperature remained below 400 °C. The minor increase in the lattice parameter may further indicate that part of Mn^{4+} was reduced to form Mn^{3+} with a larger ionic radius (0.72 *vs*. 0.67 Å, respectively, when 6 coordinate).[44]

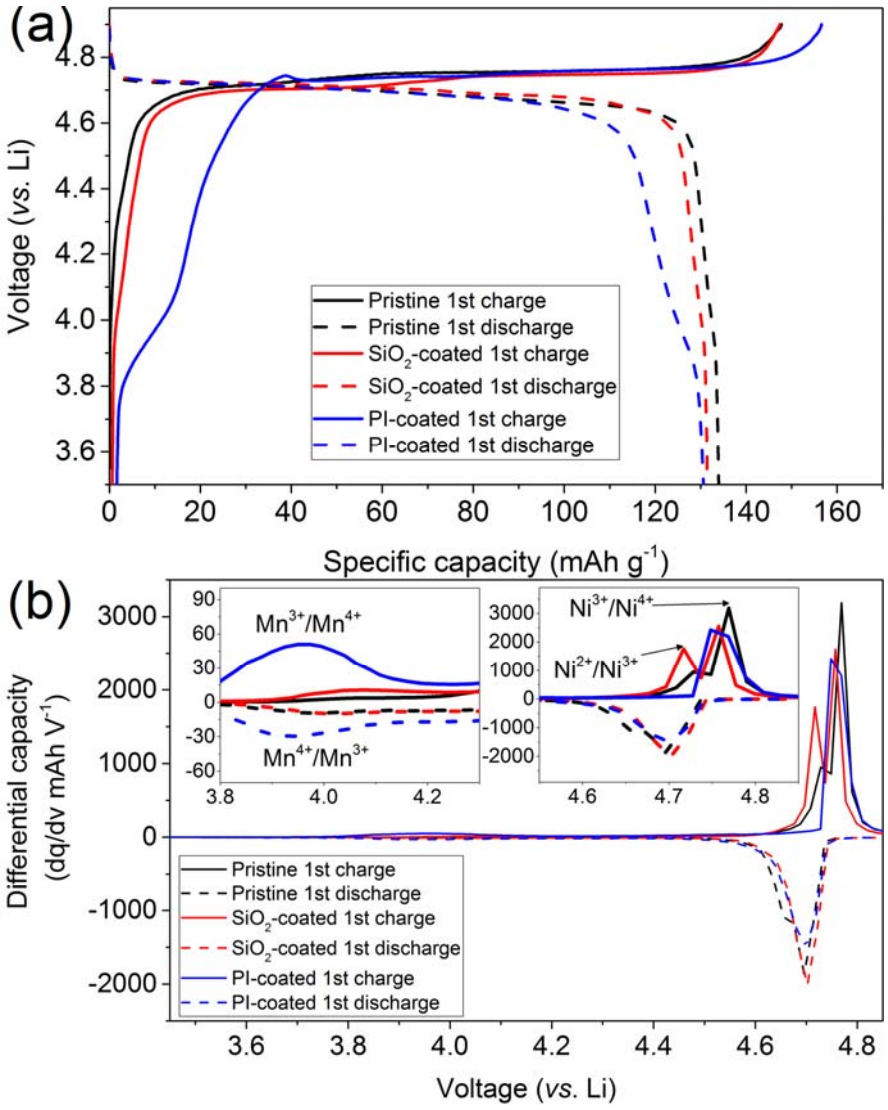

Figure 3. (a) First charge-discharge curve and (b) incremental capacity plot of coin cells containing pristine and coated P-LNMO electrodes.

Capacity retention of cells containing the different P-LNMO electrodes cycled at 0.1 C at 25 and 55 °C is shown in **Figure 4** and a summary of electrochemical performance is shown in **Table 2**. The initial discharge capacity of pristine, SiO_2-coated, and PI-coated P-LNMO at 25 °C was 130.4, 133.3, and 124.9 mAh g^{-1}, respectively, increasing at 55 °C to 134.9, 135.2, and

126.7 mAh g^{-1}, respectively. The values for the pristine P-LNMO are comparable with those reported previously.[45] The enhancement of capacity with temperature is due to higher mobility of Li^+. SiO_2-coated P-LNMO exhibits the highest capacity, likely as a result of enhanced ionic and electronic conductivities. Conversely, PI-coated P-LNMO exhibits the lowest initial discharge capacity, likely as a consequence of the non-conductivity of the PI.

At 25 °C, the pristine P-LNMO shows a capacity fade rate of 0.0363 mAh g^{-1} $cycle^{-1}$, whilst the lower capacity fade rate of 0.0197 mAh g^{-1} $cycle^{-1}$ was observed for the SiO_2-coated P-LNMO and a higher capacity fade rate of 0.0515 mAh g^{-1} $cycle^{-1}$ was found for PI-coated P-LNMO. Remarkably, the SiO_2 coating reduced the capacity fade rate by almost a factor of two, indicating the successful protection of P-LNMO from hydrofluoric acid attack. We note that PI-coated P-LNMO underwent anomalous and unstable processes in the first 13 cycles before stabilizing. The origin of this early instability is unknown and has not been observed in other polymer-coated materials, although it is possible that the PI coating initially blocks Li diffusion and a growing SEI layer offers "tunnels" for Li diffusion in the following cycles.

At 55 °C, the cycling performance of pristine P-LNMO is particularly poor, exhibiting a capacity fade rate of 0.3928 mAh g^{-1} $cycle^{-1}$. At such temperatures the organic electrolyte more readily decomposes at high voltages,[12-17] forming a SEI layer with low lithium conductivity and hindering rate capability.[21-22] Hydrofluoric acid formed from the electrolyte decomposition corrodes the P-LNMO and accelerates the dissolution of Mn into the electrolyte. The SiO_2 layer effectively mitigated capacity fade, which reduced by ~ 65%. This better cycling performance is not only attributed to the reduced direct contact between P-LNMO particles and the electrolyte, but also to the enhanced Li^+ diffusivity through the SiO_2 layer. The PI coating reduced capacity

fade at 55 °C by ~ 85%, likely as a consequence of the excellent thermal stability, good chemical resistance, and mechanical properties of the PI, which very effectively modulate capacity fade.

It is known that the electrochemical performance of the electrodes can vary with cell construction and preparation method, leading to difficulty in comparing the effects of coatings on P-LNMO to those reported for F-LNMO. Hence, results are compared by considering the effect of coatings relative to the pristine LNMO. SiO_2-coated F-LNMO is found to deliver ~ 96% of the capacity of the pristine F-LNMO and enhance capacity retention after 100 cycles at 55 °C by ~ 37% .[32] This is significantly lower than the ~ 65% enhancement by the SiO_2 coating that we find for P-LNMO, suggesting a greater benefit for high-temperature capacity fade of the SiO_2 coating for P-LNMO relative to F-LNMO. PI-coated F-LNMO is reported to have a similar capacity retention to uncoated F-LNMO at 25 °C, but a ~ 22% higher capacity retention than uncoated F-LNMO at 55 °C after 50 cycles at 1 C.[40] This is also significantly poorer than the ~ 85% enhancement to capacity retention induced by PI coating for P-LNMO. Therefore, whilst the SiO_2 and PI coatings reduce the capacity fade rate of both P-LNMO and F-LNMO, the reduction is more pronounced for P-LNMO. This is an interesting result given that P-LNMO undergoes two two-phase reactions during LIB operation in contrast to the solid-solution and single two-phase reaction of F-LNMO,[18, 20] where the capacity fade is generally associated with two-phase reactions that lead to particle segregation and pulverization. Although the SiO_2 and PI coatings do not change the mechanistic behavior of LNMO, they may act to suppress particle segregation.

Table 2. Summary of cycling performance at 25 and 55 °C.

	Electrochemical performance	Pristine	SiO_2-coated	PI-coated
25 °C	Initial specific discharge capacity (mAh g^{-1})	130.4	133.3	124.9

55 °C	Capacity fade rate (mAh g^{-1} $cycle^{-1}$)	0.0363	0.0197	0.0515*
	Initial specific discharge capacity (mAh g^{-1})	134.9	135.2	126.7
	Capacity fade rate (mAh g^{-1} $cycle^{-1}$)	0.3928	0.1371	0.0585

* Calculated after the 14th cycle.

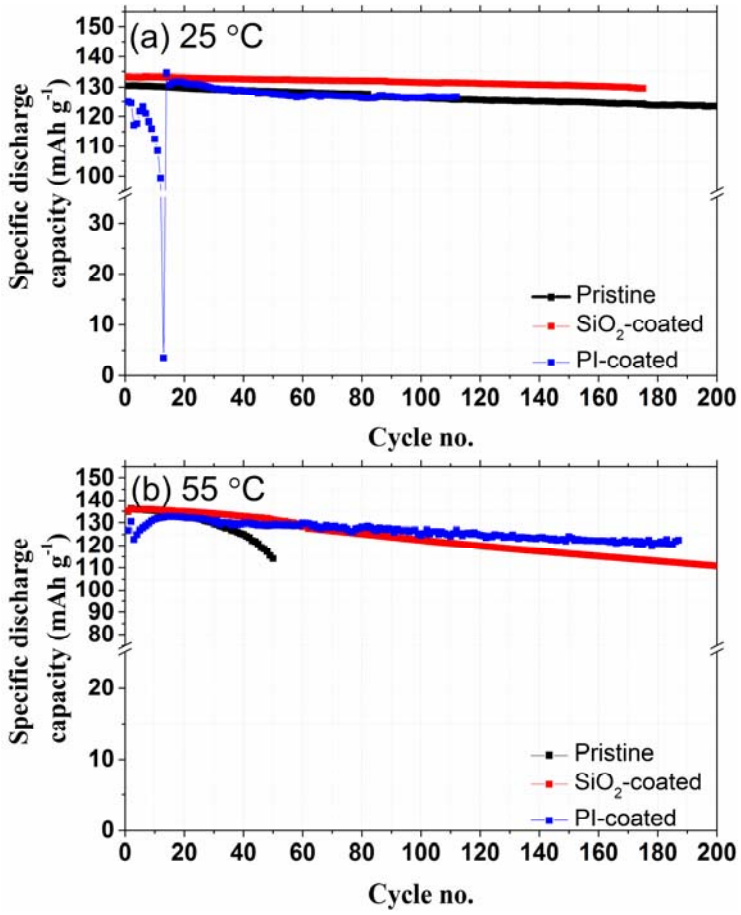

Figure 4. Cycling performance of pristine, SiO_2-, and PI-coated P-LNMO in coin cells at 0.1 C at (a) 25 and (b) 55 °C.

We also find that the coatings have pronounced effects on the P-LNMO rate capability. **Figure 5** and **6** show the charge-discharge curves at various C rates for coin-cells containing P-LNMO, and a summary of their rate capability for specific discharge capacity and energy density,

respectively. As shown in **Figure 6a**, the specific discharge capacity of pristine P-LNMO reaches 135.7 mAh g^{-1} at 0.1 C and remains > 119.2 mAh g^{-1} up to 10 C, which is significantly better than some reported values,[35, 46-48] but drops to 56 mAh g^{-1} when the C rate increases to 20 C. This excellent rate capability is also observed in the SiO_2-coated P-LNMO, which exhibits a discharge capacity of 94.7 mAh g^{-1} at 20 C, likely as a result of the enhanced ionic and electric conductivities. In contrast, the PI-coated P-LNMO shows poorer capacity performance, being 131.9 mAh g^{-1} at 0.1 C and 106 mAh g^{-1} at 10 C, and dropping to 60.5 mAh g^{-1} at 20 C. We also find that the rate-induced polarization is severe in the case of the pristine and PI-coated P-LNMO, leading to the reduction of specific energy density performance (**Figure 6b**). At 20 C, the SiO_2-coated P-LNMO retains ~ 61.0% of its specific energy density, whilst the pristine and PI-coated P-LNMO have only ~ 32.4 and 36.9%, respectively, of their specific energy densities at 0.1 C. We note that pristine P-LNMO does not have a conductive coating such as carbon or graphite, and that the SiO_2 coating greatly reduced the rate-induced polarization, showing better energy efficiency at high rate. In terms of energy efficiency, the SiO_2-coating was found to have the greatest positive contribution to the P-LNMO. In general, the rate capability of P-LNMO is inferior to that of F-LNMO, with this attributed to strain resulting from an additional phase transition as well as lower ionic/electronic conductivity.[49]

We find that the PI coating results in slightly worse rate capability of the P-LNMO, with the PI coated material exhibiting ~ 83% of its 1 C capacity at 10 C, compared with 90 % for the uncoated material. A similar case is found for the F-LNMO, where PI coated F-LNMO retained 56% of its 1 C capacity at 10 C compared with 63% for the uncoated material.[40] This comparison also reveals that the decrease in rate capability induced by the PI is ~ 8% for P-LNMO and ~

11% for F-LNMO, although it is worth noting that the rate capability of P-LNMO is significantly better than for F-LNMO.

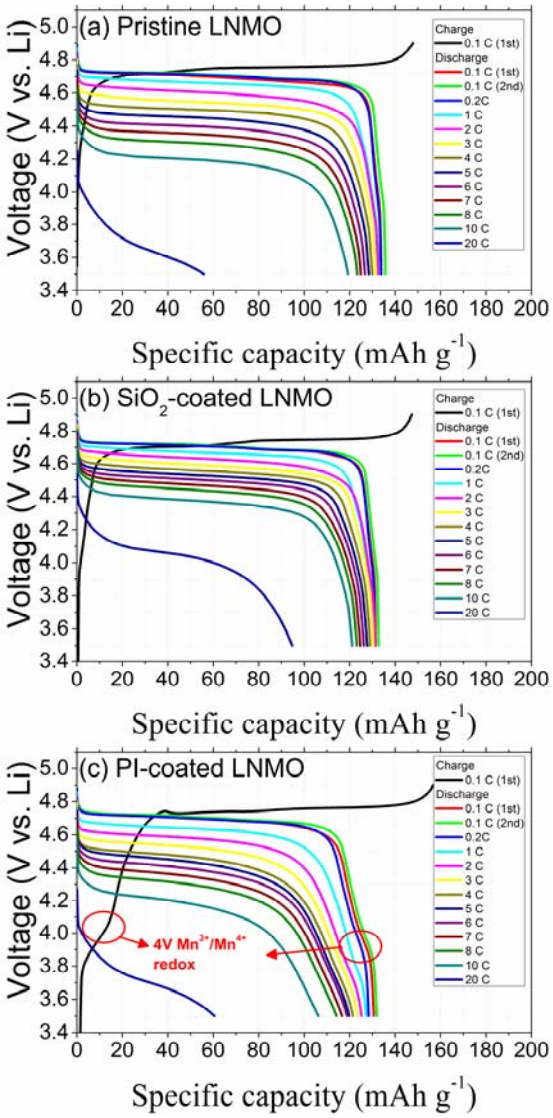

Figure 5. Charge-discharge curves of coin cells containing (a) pristine, (b) SiO_2-coated, and (c) PI-coated P-LNMO at various C rates at 25 °C.

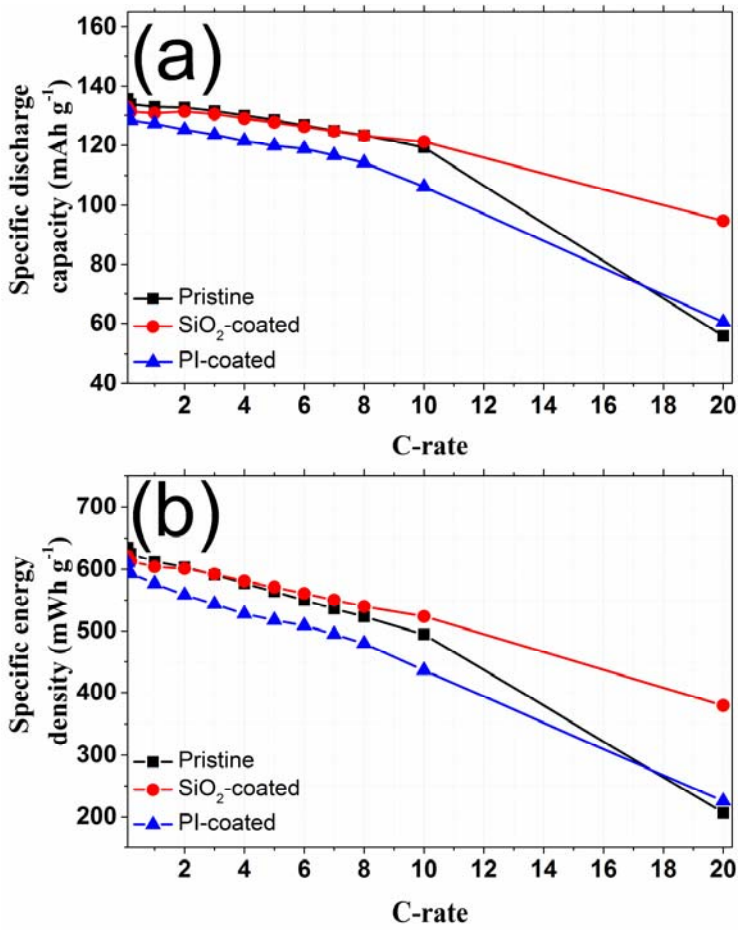

Figure 6. (a) Specific discharge capacity and (b) specific energy density as a function of C-rate for pristine, SiO_2-coated, and PI-coated P-LNMO in coin-cells.

Figure 7 shows SEM images of electrode surfaces before and after 50 cycles. Prior to cycling, the electrode surface of the three samples are smooth, and post cycling no significant changes to the electrode surface occur, indicating an absence of hydrofluoric acid attack or pulverization.

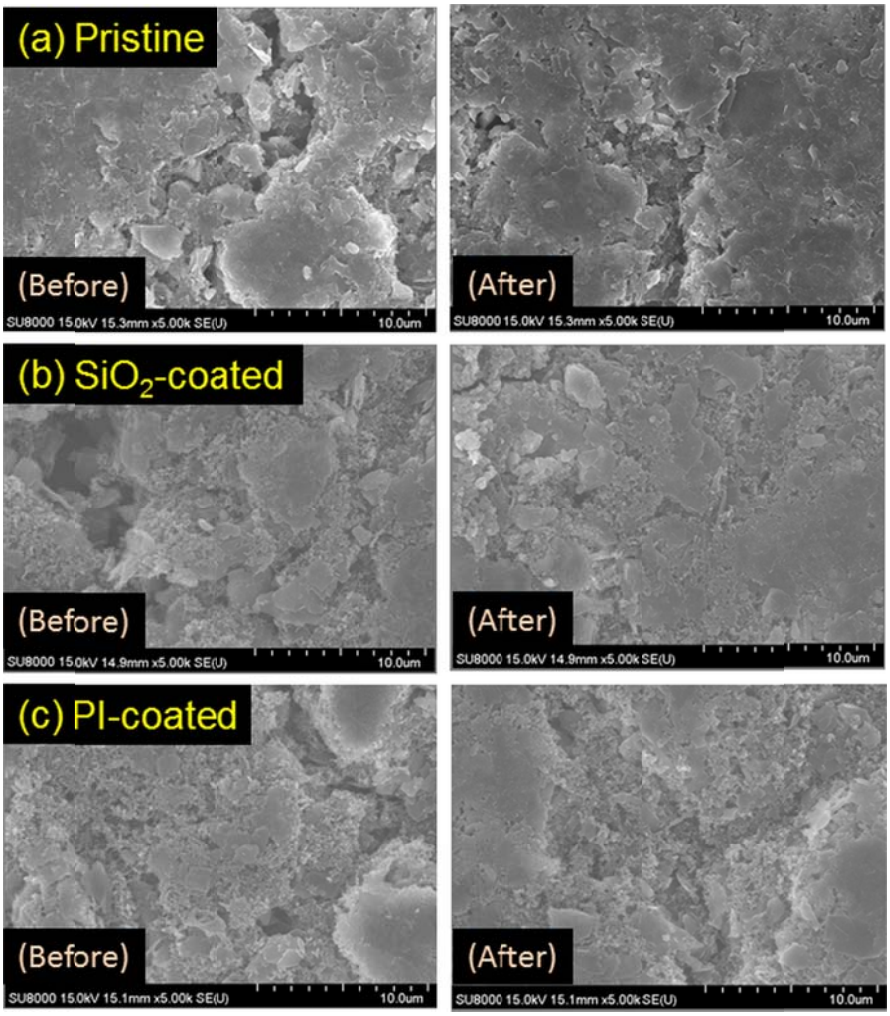

Figure 7. SEM images of electrode surfaces before and after cycling for (a) pristine, (b) SiO_2-coated, and (c) PI-coated P-LNMO at room temperature.

Electrochemical impedance spectra for the pristine and coated P-LNMO are shown in **Figure 8a** using an equivalent circuit, where fitted values are given in **Table 2**. The equivalent circuit used is a conventional Randle's circuit where R_s is the solution resistance, R_{ct} is the charge transfer resistance, W_s is the Warburg impedance, and CPE is the constant phase element used to describe double layer capacitance and coating capacitance in the electrochemical cell wherein the Randle's circuit the total impedance (Z) can be expressed as:

$$Z = R_s + R_{ct} + \sigma_w \omega^{-1/2}$$

where σ_w is the Warburg factor ($\Omega\ s^{-1/2}$) obtained by the slope of the regression line in **Figure 8b.**

The solution resistances in the three cells with various P-LNMO are similar (~ 3 Ω) as a result of these having the same electrolyte. The charge transfer resistance can be represented by the radius of the semicircle in the medium frequency range. The cycled cell containing pristine P-LNMO exhibits a R_{ct} as high as 51.4 Ω, where the cells containing SiO_2- and PI-coated P-LNMO exhibit a R_{ct} of only 11.0 and 43.9 Ω, respectively, which are ~ 21% and 85%, respectively, of that for the pristine P-LNMO cell. The fitted values for R_{ct} suggest that the SiO_2 coating significantly lowers the energy barrier for charge transfer between the electrolyte and electrode, a major cause of the rate-induced decrease in polarization. We note that the cells tested using EIS were at their discharged state-of-charge (SOC = 0%), where the material should be the least electronically and ionically conductive.[45]

The Warburg impedance can be represented in the low frequency region and is used to describe the diffusion of lithium toward or away from the electrode surface. The lithium diffusion coefficient (D_{Li}) was calculated and summarized in **Table 3**:

$$D_{Li} = \frac{1}{2}\left(\frac{RT}{n^2 A C \sigma_w F^2}\right)^2$$

where T is the temperature (298.15 K), R is the gas constant (8.314 J K^{-1} mol^{-1}), n is number of electrons per molecule during the redox reaction (1), A is the geometrical surface area[50] of the electrode (1.70 cm^2, where the diameter of the electrode is 1.47 cm), F is the Faraday constant (96485 s A mol^{-1}), and C is the bulk concentration of Li in the electrode (mol cm^{-3}, obtained using molecular volume from **Table 1**).

D_{Li} are 1 – 3 orders of magnitude lower than previously reported,[25-26, 51-53] likely as a result of the 0% SOC.[45] As similar to that for F-LNMO, at a deeper discharge state D_{Li} can be small. In this work, we compared the three LNMO electrodes and found that in the cycled cell containing SiO_2-coated P-LNMO exhibits a D_{Li} of ~ 1.4×10^{-14} cm^2 s^{-1}, which is ~ 15% higher than for the pristine P-LNMO. The cell containing PI-coated LNMO exhibited a ~ 8% lower D_{Li} than for pristine P-LNMO. Faster lithium diffusion is expected to contribute to enhanced rate capability, as observed for the cell containing SiO_2-coated P-LNMO (**Figure 5 and 6**).

Table 3. Results of EIS fitting for the three P-LNMO.

	Pristine	**SiO_2-coated**	**PI-coated**
R_s (Ω)	3.47	2.46	2.76
R_{ct} (Ω)	51.4	11.0	43.9
D_{Li} ($\times 10^{-14}$ cm^2 s^{-1})	1.252	1.437	1.154

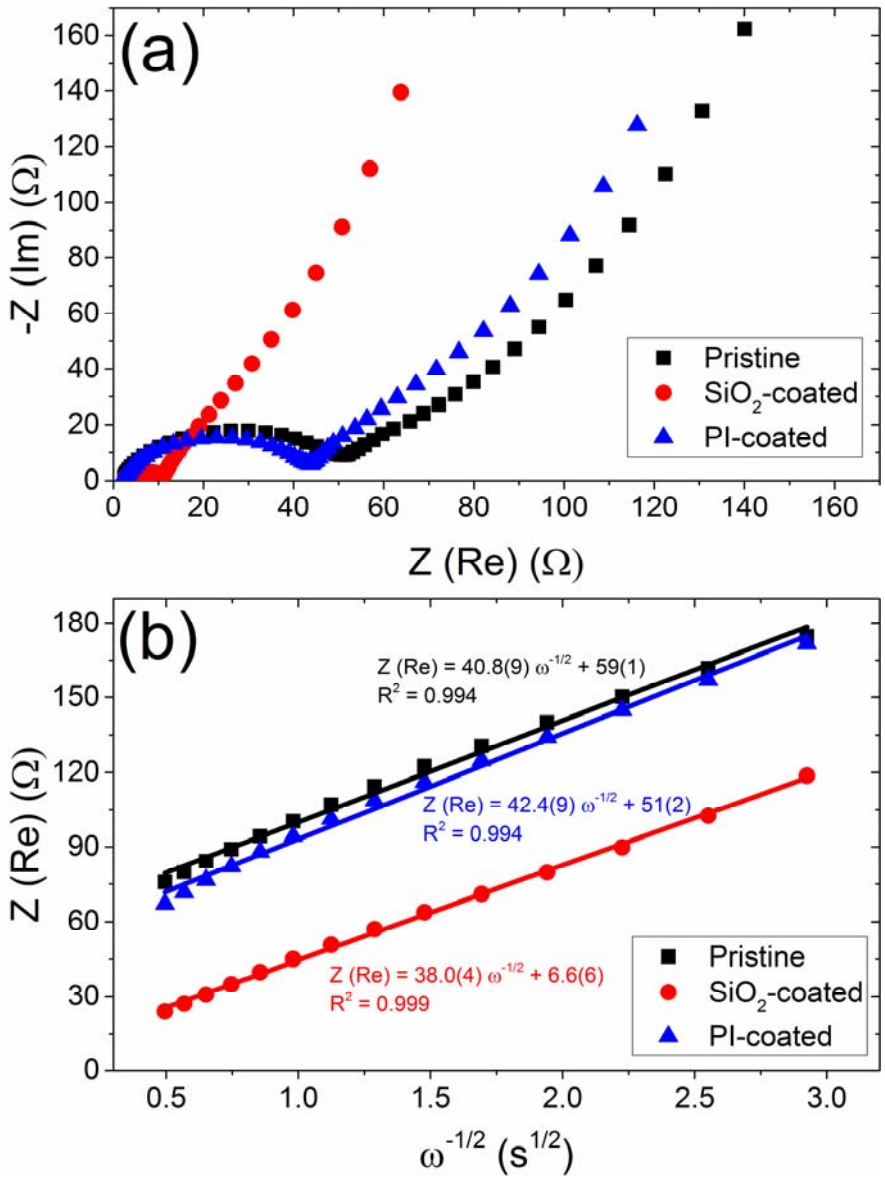

Figure 8. (a) EIS plots in the frequency range 100 kHz to 0.01 Hz, at 10 mV after 50 cycles at 0.1 C and (b) the relationship of Z (Re) and inverse square-root of angular speed for coin cells containing pristine, SiO_2-coated, and PI-coated P-LNMO.

Mn deposition on the Li electrodes in coin cells containing the different P-LNMO electrodes following 50 cycles was measured using ICP-AES, and the Mn content is shown in **Table 4**.

Although it can be seen that the Mn dissolution occurred in cells containing all three P-LNMO types, the coatings are found to provide some protection against this. The PI-coating reduced the Mn deposition by 31.3% at 25 °C and by 20% at 55 °C, relative to pristine P-LNMO, likely as a result of its good chemical resistance.

Table 4. Mn content deposited on the Li electrode in coin cells following 50 cycles.

Temperature (°C)	Mn in the Li electrode after 50 cycles (ppm)		
	Pristine	SiO_2-coated	PI-coated
25	80	62	55
55	125	103	100

■ CONCLUSIONS

High-performance transition-metal ordered $LiNi_{0.5}Mn_{1.5}O_4$ was successfully prepared using a co-precipitation method. The electrochemical performance of the ordered $LiNi_{0.5}Mn_{1.5}O_4$ was enhanced by encapsulating the particles in a thin layer of silica (SiO_2) or polyimide. The ordered $LiNi_{0.5}Mn_{1.5}O_4$ was shown to retain $P4_332$ symmetry after coating, with only a minor increase in the lattice parameter, possibly arising from the presence of Mn^{3+}. Whilst the coatings were found to not significantly affect capacity (< 5% change), they greatly affected cycling performance and rate capability. The SiO_2 coating reduced the capacity fade rate by ~ 45 and 65%, at 25 and 55 °C, respectively, whilst the polyimide coating enhanced the cycling performance by ~ 42% at 25 °C and ~ 85% at 55 °C. Further, the lithium diffusivity within the $LiNi_{0.5}Mn_{1.5}O_4$ particle was enhanced by ~ 15% by the SiO_2 coating, thereby improving rate capability up to 10 C. Whilst similar effects of these coatings are found for disordered $LiNi_{0.5}Mn_{1.5}O_4$, the magnitude of

enhancement to properties offered by these coatings is significantly less than those reported in this work for ordered $LiNi_{0.5}Mn_{1.5}O_4$. Notably, at 55 °C a SiO_2 coating enhances capacity retention by ~ 65% for the ordered material but only by ~ 37% for disordered $LiNi_{0.5}Mn_{1.5}O_4$. Similarly, a polyimide coating enhances capacity retention at 55 °C by ~ 85% for ordered $LiNi_{0.5}Mn_{1.5}O_4$ and only 22% for disordered $LiNi_{0.5}Mn_{1.5}O_4$. These differences are attributed to underlying differences in the mechanistic behavior between the ordered and disordered $LiNi_{0.5}Mn_{1.5}O_4$ phases, where the ordered material undergoes an additional two-phase reaction. A stabilizing effect of the coatings that mitigates against the phase segregation known to occur during two-phase reactions and contributes to poorer cycling performance may explain the enhanced effect for the ordered phase. This work reveals the protective effect of coatings against capacity fade for ordered $LiNi_{0.5}Mn_{1.5}O_4$ positive electrodes, which is shown to differ in magnitude to the effects offered for the $LiNi_{0.5}Mn_{1.5}O_4$ phase with disordered cations. This points to the strategic use of coatings for materials that considers not only the property of the coating, but also the reaction mechanism of the material being protected.

ASSOCIATED CONTENT

XRPD data of pristine and coated LNMO (Figure S1) and particle-size distribution measurement results of pristine LNMO (Figure S2) are included. This material is available free of charge via the Internet at http://pubs.acs.org.

AUTHOR INFORMATION

Corresponding Author

* Email: weikong.pang@ansto.gov.au (W.K.P.) Tel: +61 9717 7332

* Email: vanessa.peterson@ansto.gov.au (V.K.P.) Tel: +61 9717 9401

Author Contributions

The manuscript was written through contributions of all authors. All authors have given approval to the final version of the manuscript.

ACKNOWLEDGMENT

The authors are grateful to the support funded by Australian Research Council (ARC, FT160100251), Ministry of Economic Affairs (MOE), and Industrial Technology Research Institute (ITRI). We are also thankful to the staff members at the Australian Centre for Neutron Scattering, ANSTO for their operations support.

ABBREVIATIONS

NPD, neutron powder diffraction; XRPD, X-ray powder diffraction; LIB, Lithium-ion battery.

REFERENCES

1. Nishi, Y., Lithium Ion Secondary Batteries; Past 10 Years and the Future. *J. Power Sources* **2001**, *100*, 101-106.
2. Amatucci, G. G.; Tarascon, J. M.; Klein, L. C., CoO_2, the End Member of the Li_xCoO_2 Solid Solution. *J. Electrochem. Soc.* **1996**, *143*, 1114-1123.
3. Thackeray, M. M.; Johnson, P. J.; de Picciotto, L. A.; Bruce, P. G.; Goodenough, J. B., Electrochemical Extraction of Lithium from $LiMn_2O_4$. *Mater. Res. Bull.* **1984**, *19*, 179-187.
4. Padhi, A. K.; Nanjundaswamy, K. S.; Goodenough, J. B., Phospho Olivines as Positive Electrode Materials for Rechargeable Lithium Batteries. *J. Electrochem. Soc.* **1997**, *144*, 1188-1194.
5. Padhi, A. K.; Nanjundaswamy, K. S.; Masquelier, C.; Okada, S.; Goodenough, J. B., Effect of Structure on the Fe^{3+}/Fe^{2+} Redox Couple in Iron Phosphates. *J. Electrochem. Soc.* **1997**, *144*, 1609-1613.
6. Fergus, J. W., Recent Developments in Cathode Materials for Lithium Ion Batteries. *J. Power Sources* **2010**, *195*, 939-954.
7. Xu, B.; Qian, D.; Wang, Z.; Meng, Y. S., Recent Progress in Cathode Materials Research for Advanced Lithium Ion Batteries. *Mater. Sci. Eng. R* **2012**, *73*, 51-65.
8. Nitta, N.; Wu, F.; Lee, J. T.; Yushin, G., Li-Ion Battery Materials: Present and Future. *Materials Today* **2015**, *18*, 252-264.
9. Li, H.; Wang, Y.; Yang, X.; Liu, L.; Chen, L.; Wei, J., Improved Electrochemical Performance of 5 V $LiCoPO_4$ Cathode Materials Via Yttrium Doping. *Solid State Ionics* **2014**, *255*, 84-88.
10. Kraytsberg, A.; Ein-Eli, Y., Higher, Stronger, Better…a Review of 5 Volt Cathode Materials for Advanced Lithium-Ion Batteries. *Adv. Energy Mater.* **2012**, *2*, 922-939.
11. Manthiram, A.; Chemelewski, K.; Lee, E.-S., A Perspective on the High-Voltage $LiNi_{0.5}Mn_{1.5}O_4$ Spinel Cathode for Lithium-Ion Batteries. *Energy Environ. Sci.* **2014**, *7*, 1339-1350.
12. Tan, S.; Ji, Y. J.; Zhang, Z. R.; Yang, Y., Recent Progress in Research on High-Voltage Electrolytes for Lithium-Ion Batteries. *ChemPhysChem* **2014**, *15*, 1956-1969.
13. Kanamura, K., Anodic Oxidation of Nonaqueous Electrolytes on Cathode Materials and Current Collectors for Rechargeable Lithium Batteries. *J. Power Sources* **1999**, *81–82*, 123-129.
14. Goodenough, J. B.; Park, K.-S., The Li-Ion Rechargeable Battery: A Perspective. *J. Am. Chem. Soc.* **2013**, *135*, 1167-1176.
15. Goodenough, J. B.; Kim, Y., Challenges for Rechargeable Batteries. *J. Power Sources* **2011**, *196*, 6688-6694.
16. Goodenough, J. B.; Kim, Y., Challenges for Rechargeable Li Batteries. *Chem. Mater.* **2010**, *22*, 587-603.
17. Yang, L.; Ravdel, B.; Lucht, B. L., Electrolyte Reactions with the Surface of High Voltage $LiNi_{0.5}Mn_{1.5}O_4$ Cathodes for Lithium-Ion Batteries. *Electrochem. Solid-State Lett.* **2010**, *13*, A95-A97.
18. Pang, W. K.; Sharma, N.; Peterson, V. K.; Shiu, J.-J.; Wu, S.-H., In-Situ Neutron Diffraction Study of the Simultaneous Structural Evolution of a $LiNi_{0.5}Mn_{1.5}O_4$ Cathode and a $Li_4Ti_5O_{12}$ Anode in a $LiNi_{0.5}Mn_{1.5}O_4||Li_4Ti_5O_{12}$ Full Cell. *J. Power Sources* **2014**, *246*, 464-472.
19. Cai, L.; Liu, Z.; An, K.; Liang, C., Unraveling Structural Evolution of $LiNi_{0.5}Mn_{1.5}O_4$ by in Situ Neutron Diffraction. *J. Mater. Chem. A* **2013**, *1*, 6908-6914.

20. Ariyoshi, K.; Iwakoshi, Y.; Nakayama, N.; Ohzuku, T., Topotactic Two-Phase Reactions of $Li[Ni_{1/2}mn_{3/2}]O_4$ ($P4_332$) in Nonaqueous Lithium Cells. *J. Electrochem. Soc.* **2004**, *151*, A296-A303.
21. Talyosef, Y.; Markovsky, B.; Salitra, G.; Aurbach, D.; Kim, H. J.; Choi, S., The Study of $Lini_{0.5}mn_{1.5}o_4$ 5-V Cathodes for Li-Ion Batteries. *J. Power Sources* **2005**, *146*, 664-669.
22. Duncan, H.; Duguay, D.; Abu-Lebdeh, Y.; Davidson, I. J., Study of the $Lini_{0.5}mn_{1.5}o_4$/Electrolyte Interface at Room Temperature and 60°C. *J. Electrochem. Soc.* **2011**, *158*, A537-A545.
23. Pasero, D.; Reeves, N.; Pralong, V.; West, A. R., Oxygen Nonstoichiometry and Phase Transitions in $Limn_{1.5}ni_{0.5}o_{4-\Delta}$. *J. Electrochem. Soc.* **2008**, *155*, A282-A291.
24. Kim, J. H.; Myung, S. T.; Yoon, C. S.; Kang, S. G.; Sun, Y. K., Comparative Study of $Lini_{0.5}mn_{1.5}o_{4-\Delta}$ and $Lini_{0.5}mn_{1.5}o_4$ Cathodes Having Two Crystallographic Structures: Fd-3m and $P4_332$. *Chem. Mater.* **2004**, *16*, 906-914.
25. Kunduraci, M.; Al-Sharab, J. F.; Amatucci, G. G., High-Power Nanostructured $Limn_{2-x}ni_xo_4$ High-Voltage Lithium-Ion Battery Electrode Materials: Electrochemical Impact of Electronic Conductivity and Morphology. *Chem. Mater.* **2006**, *18*, 3585-3592.
26. Kunduraci, M.; Amatucci, G. G., The Effect of Particle Size and Morphology on the Rate Capability of 4.7 V $Limn_{1.5+\Delta}ni_{0.5-\Delta}o4$ Spinel Lithium-Ion Battery Cathodes. *Electrochim. Acta* **2008**, *53*, 4193-4199.
27. Feng, X. Y.; Shen, C.; Fang, X.; Chen, C. H., Synthesis of $Lini_{0.5}mn_{1.5}o_4$ by Solid-State Reaction with Improved Electrochemical Performance. *J. Alloy Compd.* **2011**, *509*, 3623-3626.
28. Kim, J.-H.; Yoon, C. S.; Myung, S.-T.; Prakash, J.; Sun, Y.-K., Phase Transitions in $Li_{1-\Delta}ni_{0.5}mn_{1.5}o_4$ During Cycling at 5 V. *Electrochem. Solid-State Lett.* **2004**, *7*, A216-A220.
29. Kim, C. A.; Choi, H. J.; Lee, J. H.; Yoo, S. Y.; Kim, J. W.; Shim, J. H.; Kang, B., Influence of Surface Modification on Electrochemical Performance of High Voltage Spinel Ordered-$Lini_{0.5}mn_{1.5}o_4$ Exposed to 5.3 V for 100 H before and after Surface Modification with Ald Method. *Electrochim. Acta* **2015**, *184*, 134-142.
30. Shi, J. Y.; Yi, C.-W.; Kim, K., Improved Electrochemical Performance of $Alpo_4$-Coated $Lini_{0.5}mn_{1.5}o_4$ Electrode for Lithium-Ion Batteries. *J. Power Sources* **2010**, *195*, 6860-6866.
31. Noguchi, T.; Yamazaki, I.; Numata, T.; Shirakata, M., Effect of Bi Oxide Surface Treatment on 5 V Spinel $Lini_{0.5}mn_{1.5-x}ti_xo_4$. *J. Power Sources* **2007**, *174*, 359-365.
32. Fan, Y.; Wang, J.; Tang, Z.; He, W.; Zhang, J., Effects of the Nanostructured Sio_2 Coating on the Performance of $Lini_{0.5}mn_{1.5}o_4$ Cathode Materials for High-Voltage Li-Ion Batteries. *Electrochim. Acta* **2007**, *52*, 3870-3875.
33. Sun, Y.-K.; Lee, Y.-S.; Yoshio, M.; Amine, K., Synthesis and Electrochemical Properties of Zno-Coated $Lini_{0.5}mn_{1.5}o_4$ Spinel as 5 V Cathode Material for Lithium Secondary Batteries. *Electrochem. Solid-State Lett.* **2002**, *5*, A99-A102.
34. Chong, J.; Xun, S.; Song, X.; Liu, G.; Battaglia, V. S., Surface Stabilized $Lini_{0.5}mn_{1.5}o_4$ Cathode Materials with High-Rate Capability and Long Cycle Life for Lithium Ion Batteries. *Nano Energy* **2013**, *2*, 283-293.
35. Fang, X.; Ge, M.; Rong, J.; Zhou, C., Graphene-Oxide-Coated $Lini_{0.5}mn_{1.5}o_4$ as High Voltage Cathode for Lithium Ion Batteries with High Energy Density and Long Cycle Life. *J. Mater. Chem. A* **2013**, *1*, 4083-4088.
36. Deng, Y.-F.; Zhao, S.-X.; Xu, Y.-H.; Nan, C.-W., Effect of Temperature of $Li_2o–Al_2o_3–Tio_2–P_2o_5$ Solid-State Electrolyte Coating Process on the Performance of $Lini_{0.5}mn_{1.5}o_4$ Cathode Materials. *J. Power Sources* **2015**, *296*, 261-267.

37. Shin, W.-K.; Lee, Y.-S.; Kim, D.-W., Study on the Cycling Performance of $Lini_{0.5}mn_{1.5}o_4$ Electrodes Modified by Reactive Sio_2 Nanoparticles. *J. Mater. Chem. A* **2014**, *2*, 6863-6869.
38. Kim, M. C.; Kim, S. H.; Aravindan, V.; Kim, W. S.; Lee, S. Y.; Lee, Y. S., Ultrathin Polyimide Coating for a Spinel $Lini_{0.5}mn_{1.5}o_4$ Cathode and Its Superior Lithium Storage Properties under Elevated Temperature Conditions. *J. Electrochem. Soc.* **2013**, *160*, A1003-A1008.
39. Seyyedhosseinzadeh, H.; Mahboubi, F.; Azadmehr, A., Estimation on Diffusion Coefficient of Lithium Ions at the Interface of $Lini_{0.5}mn_{1.5}o_4$/Electrolyte in Li-Ion Battery. *Ionics* **2015**, *21*, 335-344.
40. Cho, J.-H.; Park, J.-H.; Lee, M.-H.; Song, H.-K.; Lee, S.-Y., A Polymer Electrolyte-Skinned Active Material Strategy toward High-Voltage Lithium Ion Batteries: A Polyimide-Coated Lini0.5mn1.5o4 Spinel Cathode Material Case. *Energy & Environmental Science* **2012**, *5*, 7124-7131.
41. Liss, K.-D.; Hunter, B.; Hagen, M.; Noakes, T.; Kennedy, S., Echidna—the New High-Resolution Powder Diffractometer Being Built at Opal. *Physica B* **2006**, *385–386, Part 2*, 1010-1012.
42. Toby, B. H.; Von Dreele, R. B., Gsas-Ii: The Genesis of a Modern Open-Source All Purpose Crystallography Software Package. *J. Appl. Cryst.* **2013**, *46*, 544-549.
43. Liu, G. Q.; Wen, L.; Wang, X.; Ma, B. Y., Effect of the Impurity $Li_xni_{1-X}o$ on the Electrochemical Properties of 5 V Cathode Material $Lini_{0.5}mn_{1.5}o_4$. *J. Alloy Compd.* **2011**, *509*, 9377-9381.
44. Shannon, R., Revised Effective Ionic Radii and Systematic Studies of Interatomic Distances in Halides and Chalcogenides. *Acta Crystallogr. Sect. A* **1976**, *32*, 751-767.
45. Axmann, P.; Gabrielli, G.; Wohlfahrt-Mehrens, M., Tailoring High-Voltage and High-Performance $Lini_{0.5}mn_{1.5}o_4$ Cathode Material for High Energy Lithium-Ion Batteries. *J. Power Sources* **2016**, *301*, 151-159.
46. Fang, J.-C.; Xu, Y.-F.; Xu, G.-L.; Shen, S.-Y.; Li, J.-T.; Huang, L.; Sun, S.-G., Fabrication of Densely Packed $Lini_{0.5}mn_{1.5}o_4$ Cathode Material with Excellent Long-Term Cycleability for High-Voltage Lithium Ion Batteries. *J. Power Sources* **2016**, *304*, 15-23.
47. Gu, Y.-J.; Li, Y.; Fu, Y.; Zang, Q.-F.; Liu, H.-Q.; Ding, J.-X.; Wang, Y.-M.; Wang, H.-F.; Ni, J., $Lini_{0.5}mn_{1.5}o_4$ Synthesized through Ammonia-Mediated Carbonate Precipitation. *Electrochim. Acta* **2015**, *176*, 1029-1035.
48. Jin, Y.-C.; Lin, C.-Y.; Duh, J.-G., Improving Rate Capability of High Potential $Lini_{0.5}mn_{1.5}o_{4-X}$ Cathode Materials Via Increasing Oxygen Non-Stoichiometries. *Electrochim. Acta* **2012**, *69*, 45-50.
49. Kim, J.-H.; Huq, A.; Chi, M.; Pieczonka, N. P. W.; Lee, E.; Bridges, C. A.; Tessema, M. M.; Manthiram, A.; Persson, K. A.; Powell, B. R., Integrated Nano-Domains of Disordered and Ordered Spinel Phases in $Lini_{0.5}mn_{1.5}o_4$ for Li-Ion Batteries. *Chem. Mater.* **2014**, *26*, 4377-4386.
50. Kodama, R.; Terada, Y.; Nakai, I.; Komaba, S.; Kumagai, N., Electrochemical and in Situ Xafs-Xrd Investigation of Nb_2o_5 for Rechargeable Lithium Batteries. *J. Electrochem. Soc.* **2006**, *153*, A583-A588.
51. Deng, Y.-F.; Zhao, S.-X.; Xu, Y.-H.; Gao, K.; Nan, C.-W., Impact of P-Doped in Spinel $Lini_{0.5}mn_{1.5}o_4$ on Degree of Disorder, Grain Morphology, and Electrochemical Performance. *Chem. Mater.* **2015**, *27*, 7734-7742.

52. Yang, J.; Han, X.; Zhang, X.; Cheng, F.; Chen, J., Spinel $Lini_{0.5}mn_{1.5}o_4$ Cathode for Rechargeable Lithium-Ion Batteries: Nano Vs Micro, Ordered Phase ($P4_332$) Vs Disordered Phase (*Fd*-3*m*). *Nano Res.* **2013**, *6*, 679-687.
53. Liu, J.; Manthiram, A., Kinetics Study of the 5 V Spinel Cathode Limn1.5ni0.5o4 before and after Surface Modifications. *J. Electrochem. Soc.* **2009**, *156*, A833-A838.

TOC Graphic